Research article

JGS
Journal of the Geological Society

https://doi.org/10.1144/jgs2025-183 | Vol. 183 | 2026 | jgs2025-183

Evaluating the utility of rare earth elements as a redox proxy: a case study from the *c.* 1.57 Ga Gaoyuzhuang Formation, North China Craton

Xi Chen[1,2*], Ying Zhou[1], Fred Bowyer[3], Colin Mettam[1], Kun Zhang[1] and Graham A. Shields[1]

[1] LOGIC, Department of Earth Sciences, University College London, London, UK
[2] School of Ocean and Earth Science, University of Southampton, Southampton, UK
[3] School of Earth and Environment, University of Leeds, Leeds, UK
XC, 0000-0003-2297-866X; YZ, 0000-0001-8825-9583; FB, 0000-0002-3130-3894; CM, 0000-0002-3639-6399; KZ, 0000-0002-4346-9525; GAS, 0000-0002-7828-3966
* Correspondence: xi.chen@soton.ac.uk

Abstract: Rare earth elements (REE) in carbonate rocks are widely used as palaeo-ocean redox proxies partly due to their perceived resistance to diagenetic alteration. However, REE can also be mobilized at low fluid/rock ratios in anoxic porewaters, potentially modifying original patterns during early diagenesis. This study assesses REE preservation in marine carbonates across four sections of the ~1.57 Ga Gaoyuzhuang Formation (Member III), spanning a negative carbon isotope excursion linked to ocean oxygenation. Shale-normalized REE patterns show a systematic transition from light REE enrichment below and within the excursion to a more seawater-like pattern above. Our findings suggest that this shift is probably related to Fe–Mn oxide dissolution during early diagenesis. The Ce anomaly trend, identified exclusively in samples exhibiting seawater-like patterns, aligns closely with the carbon isotope excursion and the emergence of multicellular eukaryotic macrofossils. We note that samples with near-seawater Sr isotope compositions do not consistently align with those exhibiting seawater-like REE patterns, with only the latter preserving a stratigraphic trend towards more negative Ce anomalies. We therefore recommend considering normalized REE patterns when interpreting REE proxies and Ce anomalies.

Supplementary material: Full REE datasets are available at https://doi.org/10.6084/m9.figshare.c.8131252

Thematic collection: This article is part of The North China Craton as a window to Earth's middle age collection available at: https://www.lyellcollection.org/topic/collections/the-north-china-craton-as-a-window-to-earths-middle-age

Received 8 September 2025; **accepted** 1 November 2025

Rare earth elements (REE) tend to substitute with minimal fractionation for calcium in carbonate rocks and so may hold valuable insights into ancient seawater chemistry (Webb and Kamber 2000; Nothdurft *et al.* 2004). In modern oceans, heavy REE (HREE) tend to form complexes with carbonate ions, whereas light REE (LREE) are more likely to adhere to particle surfaces such as Fe/Mn (oxyhydr)oxides and organic matter, leading to an enrichment of HREE in seawater (Elderfield and Greaves 1982). The relative enrichment of HREE over LREE can be lessened under reducing conditions due to the dissolution of Fe/Mn (oxyhydr) oxides or the breakdown of organic matter, as observed in the Black Sea (German *et al.* 1991). Cerium (Ce) (III) is readily oxidized to the less soluble Ce (IV), resulting in relative Ce depletion (a negative Ce anomaly) in oxic seawater (De Baar *et al.* 1985; Sholkovitz *et al.* 1994). Consequently, REE patterns, particularly Ce anomalies in carbonate rocks, have been widely used to infer seawater redox conditions through geological time (Tostevin *et al.* 2016*a*; Wallace *et al.* 2017; Zhang *et al.* 2018).

The interpretation of REE patterns and Ce anomalies is complicated by potential contamination from non-carbonate phases during the laboratory leaching procedure, as well as by diagenetic alteration. Non-carbonate phases, such as silicates, Fe–Mn oxides, phosphates and organic matter, typically have higher REE concentrations and distinct patterns, and their dissolution during leaching can obscure the primary REE signal (Zhang and Shields 2023). To address this, sequential leaching methods have been developed to isolate primary geochemical signals in carbonate rocks, while minimizing contamination from non-carbonate phases (Bailey *et al.* 2000; Zhang *et al.* 2015; Tostevin *et al.* 2016*b*; Cao *et al.* 2020; Chen and Zhou 2023). Whereas carbonate-bound REE are generally considered resistant to late diagenetic exchange (Banner *et al.* 1988), some studies suggest that REE can be remobilized in porewaters before lithification (German and Elderfield 1990; Webb *et al.* 2009). Phase partitioning experiments and fluid–rock interaction models (Zhang and Shields 2023) indicate that early diagenetic processes, such as the dissolution of REE carrier phases (e.g. Fe–Mn oxides and organic matter), may significantly impact REE distributions. However, the extent to which this remobilization during diagenesis alters original seawater REE signatures has not been subjected to rigorous testing.

The ~1.57 Ga Gaoyuzhuang (GYZ) Formation (Member III) provides an ideal case study for assessing the preservation of REE patterns and their reliability as redox proxies. Marine carbonate rocks from this formation are characterized by a notable negative carbon isotope excursion (CIE), which approximately coincides with the emergence of decimetre-scale, multicellular, eukaryotic fossils (Zhu *et al.* 2016). Multiple lines of geochemical evidence, including a stratigraphic shift to negative Ce anomalies, suggest that this CIE is linked to ocean oxygenation (Zhang *et al.* 2018; Shang *et al.* 2019; Luo *et al.* 2020; Tang *et al.* 2022; Xie *et al.* 2023; Xu *et al.* 2023). The diverse characteristics of samples (e.g. variations in carbonate content and mineralogy) across multiple sections provide a comprehensive dataset for evaluating the resilience of REE patterns, particularly Ce anomalies, to diagenetic alteration and detrital contamination.

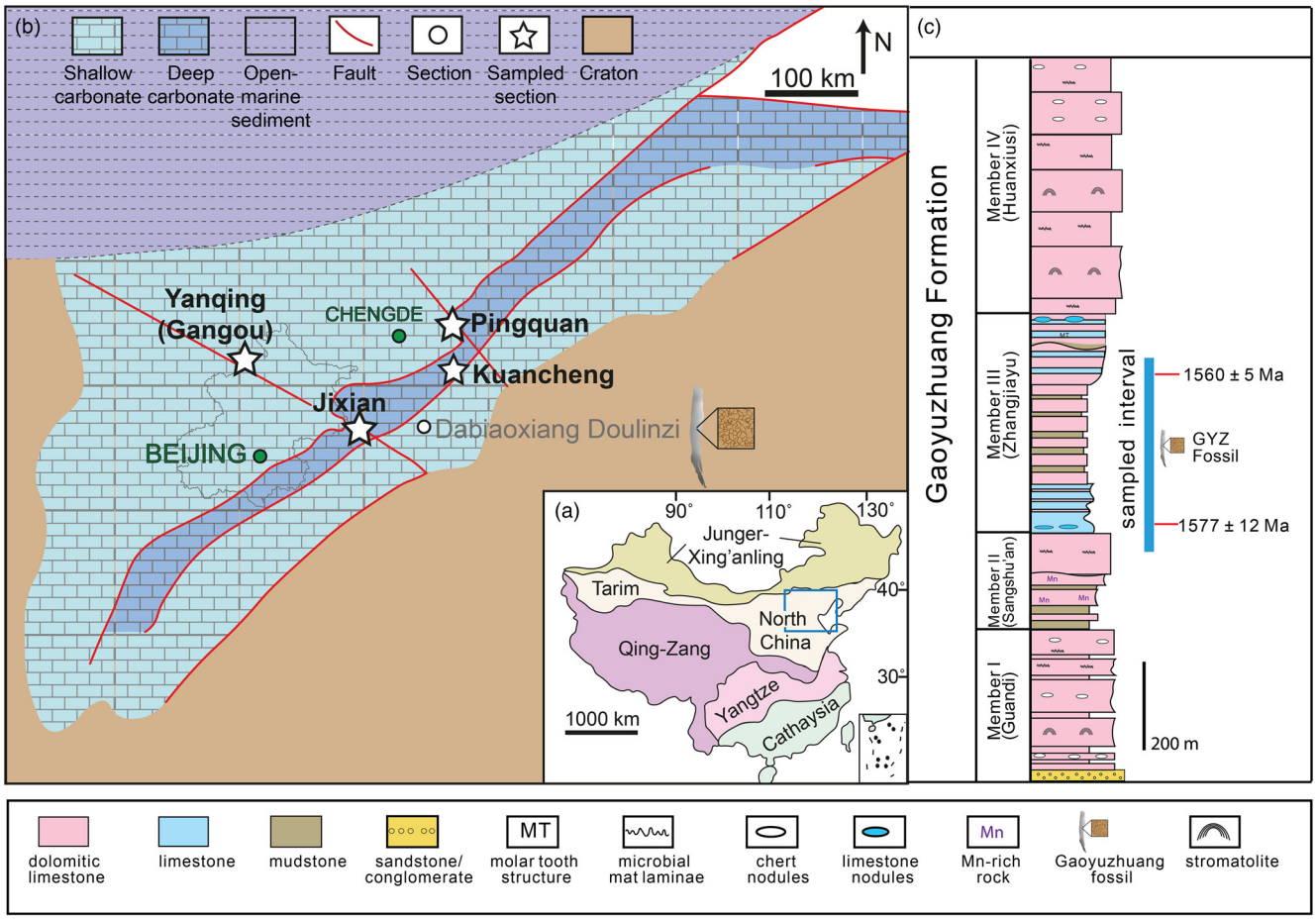

Fig. 1. Geological background of the study area. (**a**) Major tectonic subdivisions of China. The blue box shows the area shown in (b) (Yanliao Basin, North China). (**b**) Simplified Mesoproterozoic palaeogeographical map of North China during deposition of the Gaoyuzhuang Formation. The four sampled sections (shown as white stars in the map) are Jixian (40° 9′ 21.77″ N, 117° 28′ 39.69″ E), Kuancheng (40° 36′ 14.02″ N, 118° 31′ 31.75″ E), Gangou (40° 39′ 49″ N, 116° 14′ 30″ E) and Pingquan (40° 57′ 48″ N, 118° 36′ 25″ E). (**c**) General stratigraphic columns of the Gaoyuzhuang (GYZ) Formation. Source: (a) modified from Shang *et al.* (2019); (c) modified from Zhang *et al.* (2018).

In this study, we apply a sequential leaching method (Chen and Zhou 2023) to extract carbonate-bound REE data from four sections of the GYZ Formation. We investigate stratigraphic variations in REE patterns, evaluate the factors influencing their distribution, and test the fidelity of the REE data using multiple diagenetic alteration and detrital contamination indicators. Additionally, by comparing screened data with seawater-like patterns to unscreened data (the full dataset before applying any geochemical screening), we demonstrate the extent of early diagenetic overprinting on seawater REE and Ce anomaly signatures, highlighting the critical importance of fidelity checks before using REE as a redox proxy.

Geological setting

The Yanliao Basin on the North China Craton preserves an unusually complete Mesoproterozoic stratigraphic succession, with a thickness of ~9 km (Lu *et al.* 2002; Gao *et al.* 2011). The Jixian Group within the Yanliao Basin, comprising the GYZ, Yangzhuang, Wumishan, Hongshuizhuang and Tieling formations, demonstrates relatively continuous marine sedimentation, highlighted by an ~5700 m-thick marine carbonate succession in the Gaoyuzhuang to Wumishan interval (Zhang *et al.* 2018).

The GYZ Formation, dominated by marine carbonates, was deposited in deep subtidal to supratidal settings and corresponds in time to the final assembly of the supercontinent Nuna, marked by accretion on its periphery, while extensional processes may have influenced its interior (Zhang *et al.* 2012; Pourteau *et al.* 2018). The GYZ Formation is subdivided into four members: Member I (Guandi Member), Member II (Sangshu'an Member), Member III (Zhangjiayu Member) and Member IV (Huanxiusi Member) with this study focusing only on Member III (Zhangjiayu Member; Fig. 1). The lower to middle parts of Member III, with nodular limestone, thinly bedded argillaceous limestone and calcareous mudstone, indicate a deeper subtidal environment below storm wave base. The upper part, featuring 'molar tooth' limestone and microbial dolostone with ripple marks, suggests a shallower, upper subtidal to intertidal environment (Mei 2006). Two tuff beds in the lower and upper horizons of Member III yielded U–Pb zircon ages of 1577 ± 12 Ma (Tian *et al.* 2015) (Jixian section) and 1560 ± 5 Ma (Li *et al.* 2010) (Gangou section), respectively (Fig. 1c). Carbonate rocks from four sections (Pingquan, Jixian, Kuancheng, Gangou; Fig. 1b) of the GYZ Formation Member III were sampled for this study. The samples from the Gangou and Kuancheng sections are primarily dolomitic limestones, while the Pingquan and Jixian sections consist of both limestone and dolomitic limestone. Samples from the Pingquan section comprise relatively purer carbonate than those from the other sections, whereas the Gangou section is the least pure, characterized by bedded argillaceous dolomitic limestone or calcareous mudstone.

Methods

All carbonate rocks were cut to expose unweathered interiors, and the freshly cut surfaces were cleaned with compressed air and

ethanol to remove any potential surface contamination. The carbonate samples were then microdrilled, and drill sites were carefully selected to avoid veins, fractures or discoloured areas, ensuring that powders were collected from pristine material. The powdered material was collected onto clean weighing paper and transferred into acid-washed, pre-cleaned tubes. The microdrill was thoroughly cleaned between samples using compressed air and ethanol. Powdered samples were then manually ground using an agate pestle and mortar. The pestle and mortar were cleaned between samples by rinsing with deionized water to remove residual particles, followed by an ethanol rinse.

For bulk carbonate dissolution, ~10–20 mg of sample powder was dissolved in 5 ml of 2% (v/v) HNO_3 for 24 h, followed by centrifugation at 3600 rpm for 5 min. The supernatant was then collected and diluted with 2% (v/v) HNO_3 for major elemental analysis. Major element concentrations, including Ca, Mg, Mn, Fe, Al and Sr, were measured by inductively coupled plasma optical emission spectrometry (Varian 720 ICP–OES). Each data point represents the average of six replicates, with the relative standard deviation (RSD) being <3% for all the analysed elements. Standard solutions (dissolved NBS SRM 88A) were analysed to monitor analytical accuracy and precision. Measured mean concentrations for all reported major elements (Ca, Mg, Mn, Fe, Al and Sr) fell within the recommended published ranges (Gladney *et al.* 1987) with the RSDs from the repeated measurements ($n = 8$) all better than 4%. The procedural blank was included in each digestion batch. Blank Ca, Mg and Fe concentrations were less than 1% of the sample signal, while Sr, Mn and Al were consistently below detection limits, indicating negligible background contamination for all reported major elements.

Carbonate leaching experiments from Chen and Zhou (2023) have demonstrated that the first 10–30% dissolved carbonate, following prewashing, yields the most seawater-like REE pattern and highest Y/Ho ratios in argillaceous and dolomitic limestone samples from the GYZ Formation. Following this method, ~50–100 mg of micro-drilled sample powder was precleaned with 3–5 ml of 1 M ammonium acetate in an ultrasonic bath for 30 min at room temperature. After centrifugation, the residue was washed once with ultrapure water and centrifuged again. Subsequently, an amount of 0.05–0.2 M acetic acid (HAc), calculated to dissolve ~10–30% carbonate, was added to the residue. After acid addition, the samples were ultrasonically agitated for 30 min and then allowed to stand for another 30 min at room temperature, before being centrifuged at 3600 rpm for 5 min. The supernatant was collected for REE analysis. The concentrations of REE were analysed by inductively coupled plasma mass spectrometry (Agilent 7900 ICP–MS) with calibration standards (Superco, Sigma-Aldrich) and samples were matrix-matched to 50 μg g^{-1} Ca. Each data point represents the average of seven replicates, with the RSD being <5% for all the analysed elements. Standard solutions (dissolved SGR-1) were analysed to monitor analytical accuracy and precision for REE. The relative difference between the measured mean values and the published reference means (Gladney and Roelandts 1988) was less than 5% for La, Ce, Sm, Eu, Dy, Ho and Er, and less than 10% for the remaining REE. The RSD from repeated measurements of SGR-1 ($n = 4$) was better than 10% for all REE. Procedural blanks contributed less than 1% of the measured values, confirming a negligible impact on the reported REE concentrations.

All geochemical analyses were carried out at the London Geochemistry and Isotope Centre (LOGIC), University College London (UCL). REE concentrations in carbonate components were obtained by dividing the masses of REE in the leachate (HAc) by the mass of ($CaCO_3 + MgCO_3$), which is calculated based on the Ca and Mg contents in the same leachate. All reported REE concentrations in this study were normalized to post-Archean Australian Shale (PAAS: Pourmand *et al.* 2012). The La anomaly was calculated using the equation from Lawrence *et al.* (2006): $La_N/(Pr_N \times (Pr_N/Nd_N)^2)$, with N representing the normalized values. The Ce anomaly can be significantly affected by anomalous La enrichment (Bau and Dulski 1996) when it is calculated using normalized La and Pr concentrations (De Baar *et al.* 1985): $Ce/Ce^* = 2Ce_N/(La_N + Pr_N)$. To mitigate this issue, this study adopts the revised equation proposed by Lawrence *et al.* (2006) for calculating the Ce anomaly: $Ce/Ce^* = Ce_N/(Pr_N \times Pr_N/Nd_N)$. This equation replaces La with Nd to minimize artefacts caused by La variability, ensuring more reliable interpretations of redox conditions. This geometric interpolation approach is further supported by Barrat *et al.* (2023), which emphasizes its superiority over linear interpolation when calculating La and Ce anomalies.

Results

Carbon isotope values from the same samples were measured by Chen *et al.* (2025). A negative $\delta^{13}C_{carb}$ excursion was observed for three sections (Pingquan, Jixian and Gangou), showing a shift from ~ 0 to ~ −4‰, with little evidence of diagenetic overprinting (Fig. 2), consistent with previous studies of the same formation (Guo *et al.* 2013; Zhang *et al.* 2018; Shang *et al.* 2019). Due to the lack of exposure, the carbon isotope excursion is absent at the Kuancheng section. To examine REE records through the carbon isotope excursion, we divided our target interval (GYZ Member III) into four stages based on the $\delta^{13}C$ trend (Fig. 2): pre-excursion (III-1), with a mean $\delta^{13}C$ value of −0.92‰; syn-excursion (III-2), during which $\delta^{13}C$ decreases from −0.8 to −3.7‰; recovery (III-3), where $\delta^{13}C$ shifts from −3 to −0.3‰; and post-excursion (III-4), with a mean $\delta^{13}C$ value of −0.38‰. The stratigraphic correlations and age models used in this study were based on carbon isotope stratigraphy. Age tie points were selected at the peak and recovery of $\delta^{13}C$ excursions and the member boundaries. For each section, the age model was constructed by linear interpolation between tie points based on the assumption of constant sediment accumulation rates.

Modern oxic seawater typically displays shale-normalized REE patterns that feature a gradual increase in concentration from LREE to HREE, along with positive La and Gd anomalies, Ce depletion, and a super-chondritic Y/Ho ratio (Elderfield and Greaves 1982; Byrne and Kim 1990; Sholkovitz *et al.* 1994; Nozaki *et al.* 1997) (Fig. 3). Note that in the present study, the term 'seawater-like' refers to REE patterns that have similar characteristics to those of modern seawater ($Pr_N/Yb_N < 1$, La anomaly >1, $Dy_N/Sm_N > 1$ and $Y/Ho > 35$) except for Ce which is redox-sensitive. In the GYZ Formation, REE patterns change stratigraphically upwards, showing a gradual transition from LREE enrichment in lower strata (III-1) to a more seawater-like pattern in upper strata (III-4) (Figs 3, 4). Shale-normalized Pr_N/Yb_N ratios, indicative of LREE enrichment, decrease significantly from 1.56 in stage III-1 to 0.83 in stage III-4, while Dy_N/Sm_N ratios, reflecting middle REE (MREE) enrichment, increase from 0.93 in stage III-1 to 1.25 in stage III-4 (Fig. 5). The Y/Ho ratio increases from ~36 in stage III-1 to over 40 in stage III-4, and total REE concentrations (ΣREE) decline from stage III-1 to III-4, decreasing from around 85 to 46 ppm (Fig. 5). Statistical significance was evaluated using two-tailed t-tests with differences considered significant at $P < 0.05$. All parameters reported above show highly significant differences ($P < 0.001$) between stage III-1 and stage III-4.

All four sections exhibit consistent REE features across stages III-1, III-2 and III-4. The pre- and syn-excursion stages (III-1, III-2) exhibit non-seawater-like patterns with LREE enrichment, while the post-excursion stage (III-4) displays more seawater-like patterns. The only inconsistency arises in stage III-3 (the recovery stage of the excursion) between the Gangou and Pingquan sections, the two

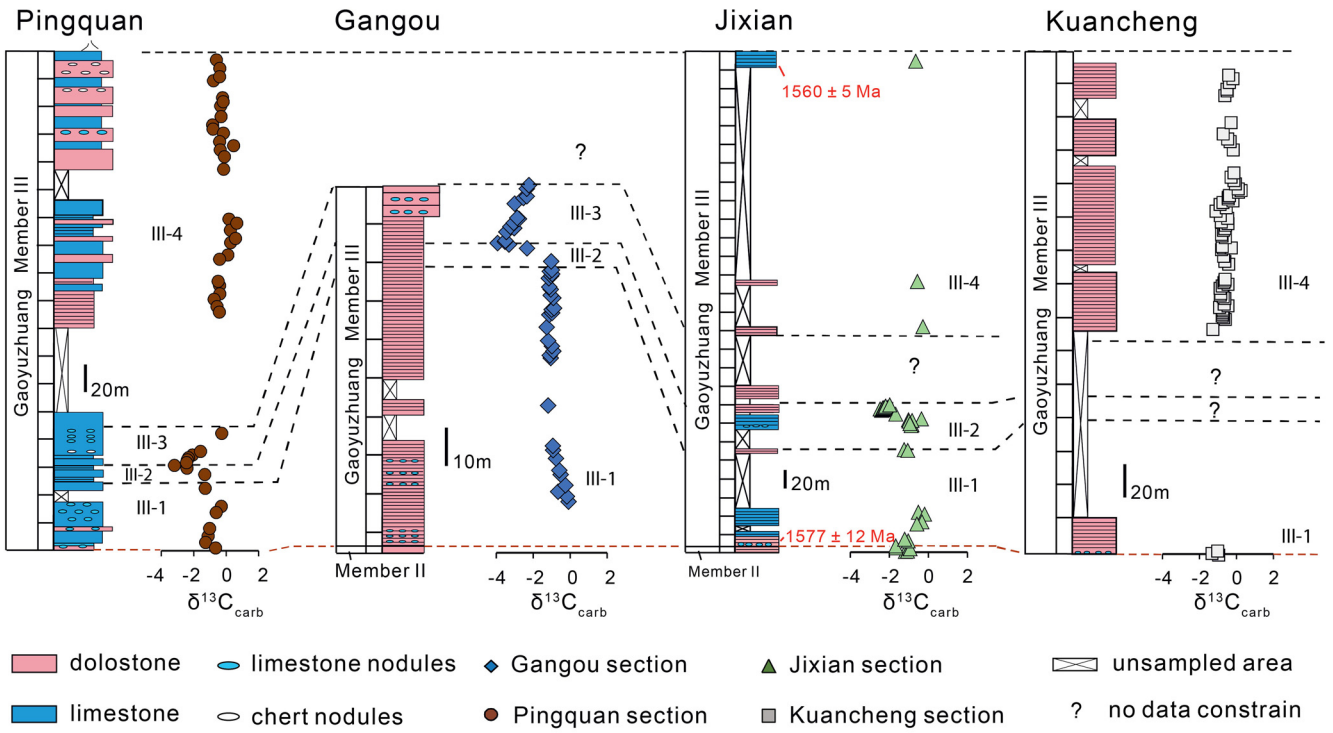

Fig. 2. Stratigraphic columns for each section of the Gaoyuzhuang Formation Member III, with divisions into four stages (III-1 to III-4) based on carbon isotope ($\delta^{13}C$, ‰) trends. The stages are: pre-excursion (III-1), syn-excursion (III-2), recovery (III-3) and post-excursion (III-4). Note that the Gangou section lacks stage III-4, the Jixian section lacks stage III-3, and the Kuancheng section lacks stages III-2 and III-3. Dashed lines indicate stage boundaries. The corresponding rare earth element patterns for each stage in each section are shown in Figure 3.

sections that captured stage III-3 (Fig. 3). In the Pingquan section, a more seawater-like pattern similar to III-4 is already apparent, whereas the Gangou section continues to show LREE enrichment, resembling the REE patterns of stages III-1 and III-2. Before screening, Ce anomaly values show no clear trend across different stages. In stage III-1, Ce anomaly values range from 0.83 to 1.15, with a mean of 0.93 ± 0.01 (1SE). Stage III-2 ranges from 0.85 to 1.02, with a mean of 0.95 ± 0.01, while stage III-3 ranges from 0.88 to 0.98, with a mean of 0.93 ± 0.01. Stage III-4 values range from 0.83 to 1.05, with a mean of 0.91 ± 0.01. Similarly, no distinct trend is observed across different sections, with all sections having a mean value of ~0.9 (Fig. 4). The full REE datasets are provided in the Supplementary Table.

Discussion

Stratigraphic REE patterns

The stratigraphic transition of REE patterns from light REE enrichment to a more seawater-like pattern is remarkable. The REE patterns in carbonate rocks can be potentially altered during sample preparation due to inadvertent leaching of non-carbonate phases (Zhang *et al.* 2015; Tostevin *et al.* 2016*b*; Cao *et al.* 2020). Nevertheless, we employed a sequential leaching method by partially dissolving less than 30% of the total carbonate with dilute HAc (0.05–0.2 M) following an ammonium acetate prewash. This method has proven effective in removing the exchangeable phase, while minimizing the dissolution of non-carbonate phases, even in argillaceous carbonate rocks (Chen and Zhou 2023). Since all samples were leached using the same method, the observed stratigraphic changes of REE patterns are unlikely to be artefacts of the leaching technique. The absence of covariation between bulk carbonate concentrations (Al, Rb, Si) and REE pattern parameters (Fig. 5b, c) also suggests that detrital phases are not the main contributors to REE alteration away from seawater-like patterns.

The non-seawater-like REE pattern may result from mixing of seawater with an unusual source (e.g. freshwater), possibly due to deposition in a non-marine or restricted environment (Kamber *et al.* 2004; Zhao *et al.* 2009; Corkeron *et al.* 2012). However, this is unlikely to explain the observed REE pattern transition because the studied interval is considered to have been deposited in a subtidal environment with good connectivity to the open ocean (Luo *et al.* 2025). The freshwater mixing scenario is also inconsistent with the appearance of seawater-like REE patterns in shallower water deposits (i.e. stage III-4; Fig. 4). On the other hand, the slope of REE patterns may be affected by seawater pH due to its impact on REE aqueous complexation (e.g. Barnes 2023; Lin and Catling 2024). Although constraints on Precambrian seawater pH remain sparse and debated, changes in seawater pH are unlikely to induce a negative slope in REE patterns (i.e. LREE relative enrichment; Lin and Catling 2024).

It has also been proposed that REE patterns dissimilar to that of modern oceans reflect distinct primary seawater chemistry (Lécuyer *et al.* 2004; Planavsky *et al.* 2010; Hood and Wallace 2015). In this scenario, relative enrichment of LREE and/or MREE over HREE is generally attributed to reductive dissolution of Fe/Mn oxides in suboxic and/or anoxic waters. While the dissolution of settling particles in reducing seawater can lessen HREE enrichment, the relative enrichment of LREE over HREE is not evident in modern anoxic seawater (Zhang and Shields 2022). Importantly, this hypothesis appears to conflict with carbonate I/(Ca + Mg) values, which would be expected to be low beneath anoxic waters. This is due to rapid iodate reduction in reducing seawater (Wong and Brewer 1977) and only iodate is incorporated into the carbonate lattice (Lu *et al.* 2010; Hashim *et al.* 2022). However, carbonate I/(Ca + Mg) values are mostly higher than 0.5 μmol mol^{-1} through the negative $\delta^{13}C_{carb}$ excursion at Gangou and Jixian (Shang *et al.* 2019; Tang *et al.* 2023), although LREE enrichment persists in the same interval (Figs 3, 4, stage III-2). Therefore, the temporal evolution of seawater chemistry is unlikely to explain the stratigraphic transition of REE patterns.

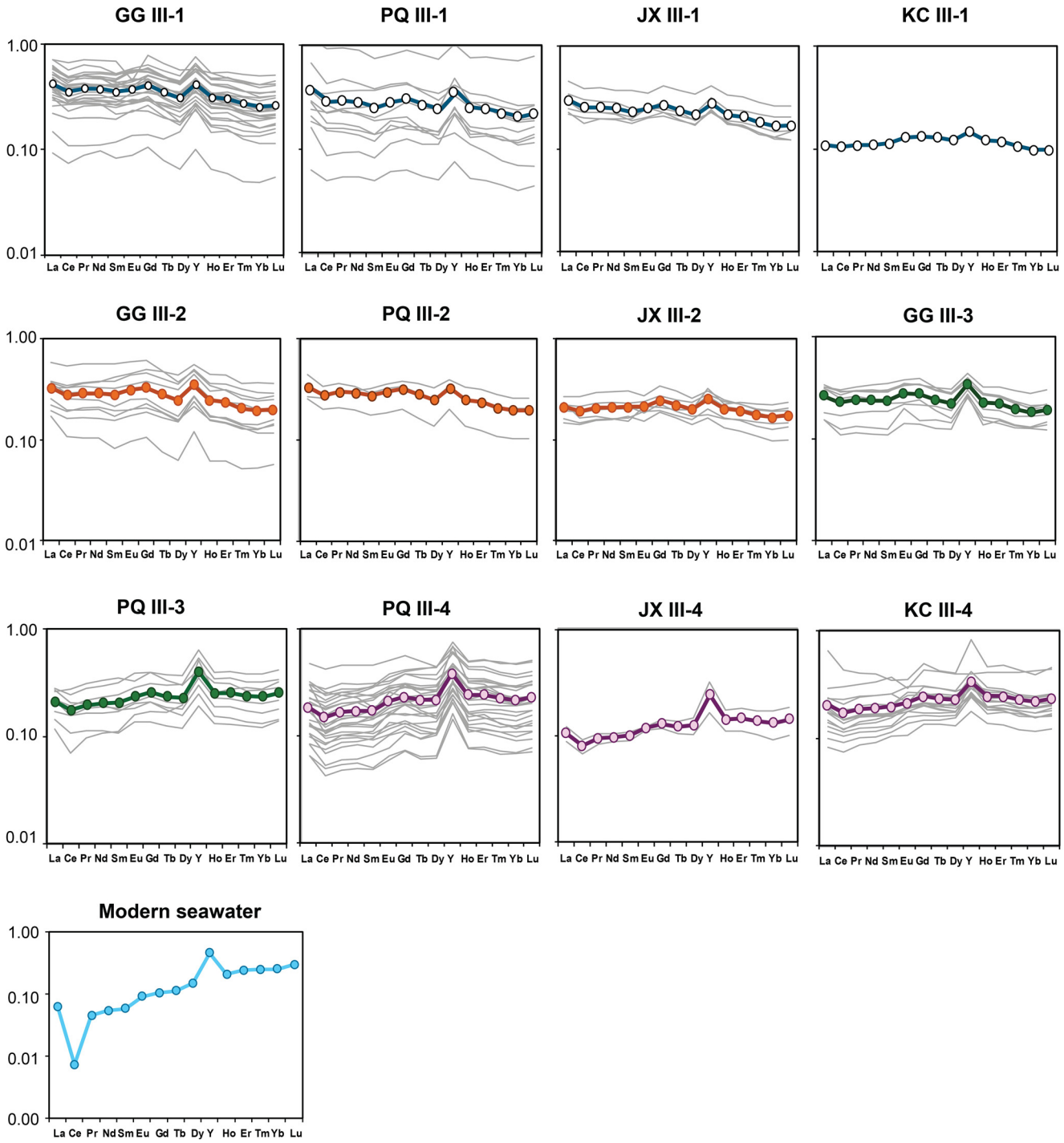

Fig. 3. Rare earth element (REE) patterns for each stage in each section (Gangou – GG, Pingquan – PQ, Kuancheng – KC, and Jixian – JX). Coloured lines with dots indicate mean values for each stage, with different colours representing different stages. All REE plots are presented with the *y*-axis on a logarithmic scale and normalized to post-Archean Australian Shale (PAAS) (Pourmand *et al.* 2012). Source: the modern seawater REE plot is from Zhang and Shields (2022), with normalized values multiplied by 10^6.

Given the lack of evidence for significant recrystallization (Zhang *et al.* 2018; Shang *et al.* 2019), it also seems unlikely that the stratigraphic REE patterns relate to late-stage diagenetic exchange. We consider therefore that the REE transition reflects the influence of early diagenetic exchange (Zhang and Shields 2023). To identify the potential diagenetic influence on REE patterns, key REE parameters (Pr_N/Yb_N, Dy_N/Sm_N and Y/Ho ratios) are plotted against ΣREE and diagenetic indicators (Fig. 5). Bulk carbonate Mn and Fe concentrations covary with REE pattern parameters (Fig. 5e–g), showing particularly strong correlations ($R^2 = 1$) with both Pr_N/Yb_N and Dy_N/Sm_N (Fig. 5e). Mn and Fe concentrations are generally elevated in reducing seawater due to oxide dissolution, and hence such a relationship may be taken to imply an overarching control from ambient redox conditions. As discussed above, given the high redox potential of iodine (Rue *et al.* 1997), relatively high carbonate I/(Ca + Mg) values argue against a strongly reducing water column (especially in Stage III-2; Shang *et al.* 2019; Tang *et al.* 2023). Mn and Fe concentrations can also be elevated in early diagenetic, anoxic porewaters, whereby iodine enrichment in carbonates may be lowered but not removed entirely, as observed in some manganese-rich carbonates (Zhang *et al.* 2025). In other words, elevated Mn and Fe concentrations in the GYZ Formation are quite

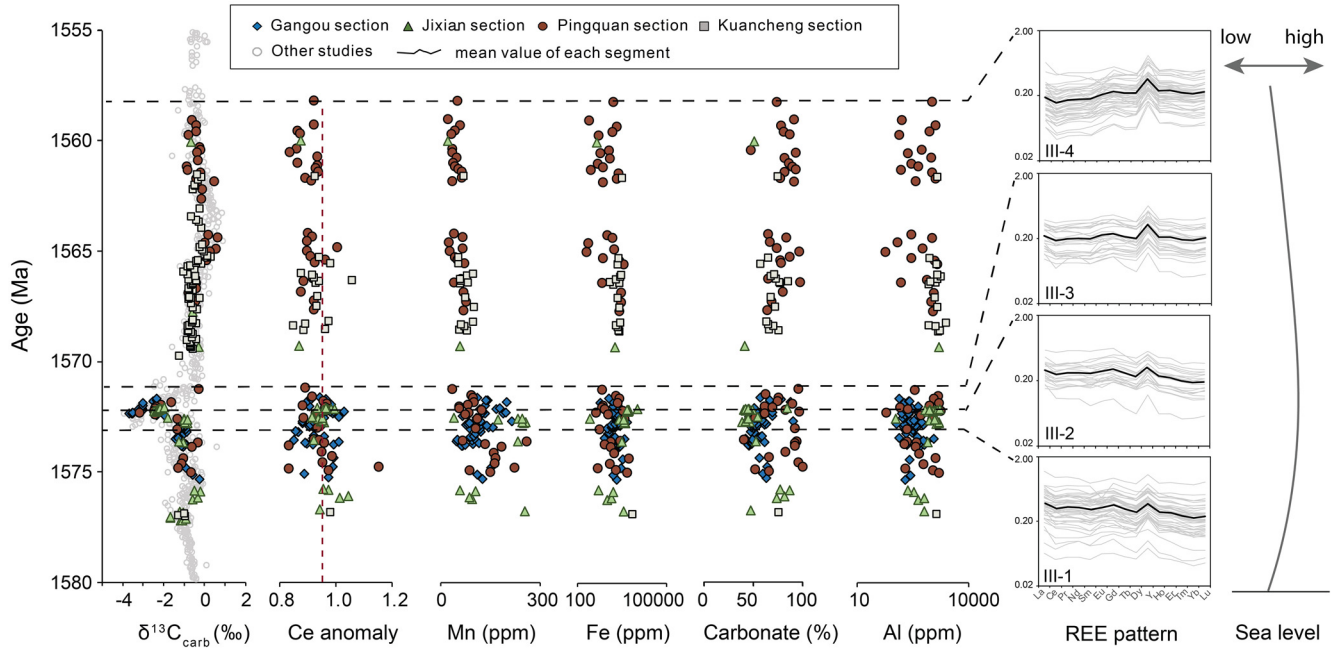

Fig. 4. Integrated stratigraphic trends of carbon isotopes, unscreened Ce anomaly, rare earth element (REE) patterns, sea-level changes, bulk carbonate Mn, Fe and Al concentrations, and carbonate content. Note that Fe and Al concentrations are shown on a log scale. The red vertical dashed line indicates the Ce anomaly at 0.95. Horizontal dashed lines indicate stage boundaries. The REE patterns presented here are integrated from four sections for each stage, with the black line indicating the mean value. Water depth shows an initial deepening trend followed by a shallowing trend (Zhang *et al.* 2018). Unscreened Ce anomalies show no distinct stratigraphic trend. Source: carbon isotopes of the Gangou, Jixian, Pingquan and Kuancheng sections are from Chen *et al.* (2025); the others (grey circles) are from Guo *et al.* (2013), Shang *et al.* (2019) and Zhang *et al.* (2018).

consistent with Fe–Mn oxide dissolution during early diagenesis. Considering that LREE and MREE are preferentially scavenged by Fe–Mn oxides (Koeppenkastrop and De Carlo 1993; Bau *et al.* 2014), the observed strong covariations may reflect the incorporation of REE from porewaters modified by the dissolution of particulate REE carrier phases, such as Fe–Mn oxides.

The dissolution of Fe and Mn oxides during early diagenesis may also explain the differences between the Gangou and Pingquan sections in stage III-3 (Fig. 3). In the Gangou section, LREE enrichment persists, while the Pingquan section exhibits a more seawater-like pattern. A positive covariation between Mn and Fe concentrations, Mg/Ca, and the HREE enrichment indicator (Pr_N/Yb_N) is observed in the Gangou section, but no such covariation exists in the Pingquan section. This suggests that early diagenetic alteration in the Gangou section is perhaps more pronounced compared with the Pingquan section during stage III-3, possibly related to lower carbonate content in the Gangou section, making it more susceptible to alteration.

It has also been proposed that REE fractionation in the GYZ Formation may be associated with the dolomitization process (Liang *et al.* 2020). We observed a weak covariation between Mg/Ca and Pr_N/Yb_N, as well as with Dy_N/Sm_N, suggesting that dolomitization may have contributed to REE redistribution to some extent, despite the relatively large error bar. Sr concentrations in the bulk rock also correlate with REE pattern parameters, decreasing as REE patterns shift towards a non-seawater signature ($Pr_N/Yb_N > 1$, $Dy_N/Sm_N < 1$, lower Y/Ho and higher ΣREE; Fig. 5k–m). Diagenesis, including dolomitization, typically increases the Mn and Fe concentrations in carbonate rocks, while decreasing Sr concentrations, due to the higher distribution coefficients of Mn and Fe in stable carbonate minerals compared to Sr (Rimstidt *et al.* 1998). Although the direct impact of dolomitization on REE patterns is difficult to quantify, it is likely that dolomitization facilitated alteration of carbonate REE patterns through interactions with LREE-enriched porewater (influenced by dissolution of particulate Fe and Mn oxides), as dolomitization involves open-system water–rock interactions and may increase rock porosity (Weyl 1960).

It is worth noting that although the average ΣREE shows some covariation with pattern parameters (Fig. 5a) and diagenetic/detrital parameters (Fig. 5d, j and m), using ΣREE as a diagenetic indicator requires caution. In this study, REE content exhibits a greater range within individual stages than between them, while REE patterns remain relatively consistent within stages (Figs 3, 4). This suggests that changes in REE content do not necessarily correspond to changes in REE patterns that might be influenced by diagenesis. Therefore, the covariations between ΣREE and pattern/diagenetic parameters across stages may also be driven by environmental conditions rather than simple diagenetic enrichment. This could also explain why the correlations between diagenetic indicators (e.g. Fe + Mn, Sr) and REE content across stages are much weaker than their correlation with REE pattern indicators.

Comparing diagenetically sensitive $^{87}Sr/^{86}Sr$ with REE patterns

Strontium isotopes ($^{87}Sr/^{86}Sr$) are traditionally used as weathering proxies and are also widely employed to indicate sample alteration due to their sensitivity to diagenesis and clay contamination (McArthur 1994; Gorokhov *et al.* 1995; Ovchinnikova *et al.* 1995). Generally, post-depositional processes tend to increase $^{87}Sr/^{86}Sr$ values because K-bearing silicates (rich in ^{87}Rb and, therefore, having higher $^{87}Sr/^{86}Sr$) release radiogenic ^{87}Sr into interstitial fluids, which can then be incorporated into carbonate rocks during diagenetic recrystallization. In contrast, fluids with less radiogenic Sr isotopes than contemporaneous seawater, influenced by mafic/juvenile magmatic silicate and/or hydrothermal fluids, may drive carbonate $^{87}Sr/^{86}Sr$ to lower values (Miller *et al.* 2008; Brand *et al.* 2010; Satkoski *et al.* 2017; Cui *et al.* 2020). Covariation between Sr isotopes and Mn/Sr, Mg/Ca and Sr/(Ca + Mg) have proven to be robust indicators of diagenetic trends and have been successfully used in numerous studies (Halverson *et al.* 2007; Cox *et al.* 2016;

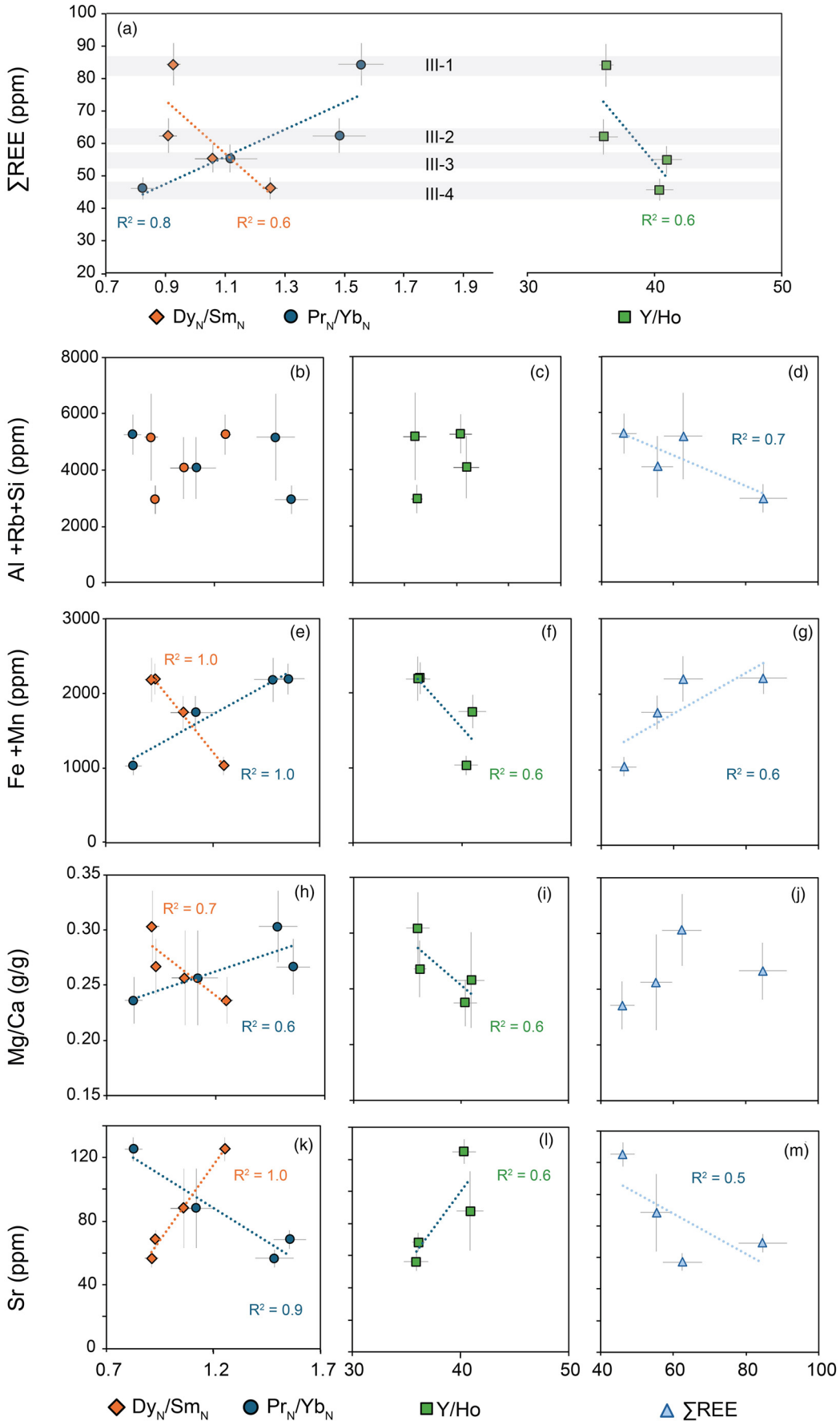

Fig. 5. Cross-plots for identifying secondary alteration in the stratigraphic changes of rare earth element (REE) patterns. All data represent the mean values of four sections in each stage, with error bars indicating the standard error. (**a**) Cross-plots of total REE concentration (ΣREE) against REE pattern-related parameters (Dy_N/Sm_N, Pr_N/Yb_N, Y/Ho) for each stage (marked by grey shading). Seawater-like patterns, such as those in stage III-4 samples, are typically characterized by lower REE concentration, lower Pr_N/Yb_N (usually <1), higher Dy_N/Sm_N (usually >1) and higher Y/Ho. (**b**–**m**). Cross-plots of detrital contamination indicators (Al + Rb + Si) and diagenetic indicators (Fe + Mn, Mg/Ca, Sr concentration) from bulk carbonate against REE pattern indicators and ΣREE. Only covariations with a correlation coefficient $R^2 > 0.5$ are shown with trend lines.

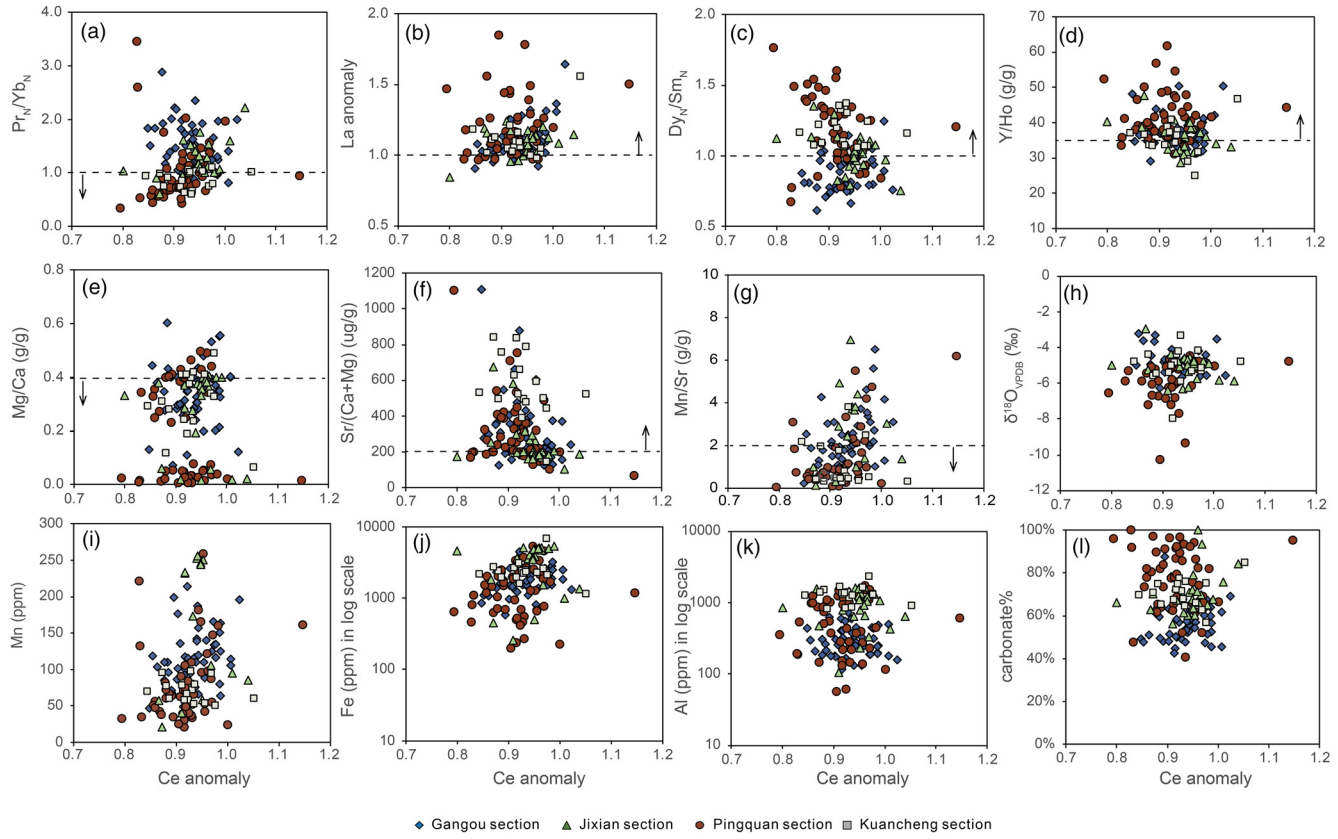

Fig. 6. Cross-plots for Ce anomaly screening for individual sections. (**a**–**d**) Cross-plots of rare earth element (REE) pattern parameters with Ce anomaly, with cut-offs set as $Pr_N/Yb_N < 1$, La anomaly >1, $Dy_N/Sm_N > 1$ and Y/Ho > 35 to select seawater pattern samples (as indicated by arrows). (**e**–**g**) Cross-plots of traditionally used diagenetic indicators for Sr isotopes with Ce anomaly, where seawater Sr isotopes of the same samples (Chen *et al.* 2025) are characterized by Mg/Ca < 0.4 g g^{-1} (<0.05 g g^{-1} for limestone), Sr/(Ca + Mg) > 200 μg g^{-1} and Mn/Sr < 2 g g^{-1} (<1 g g^{-1} for limestone) as shown by arrows. (**h**–**l**) Cross-plots of oxygen isotopes, bulk carbonate Mn, Fe and Al, and carbonate content with Ce anomaly to identify potential alteration. No covariation can be observed across all sections for any of the parameters.

Kuznetsov *et al.* 2018; Zhou *et al.* 2020). The cut-offs for these parameters are not unique, as diagenetic conditions differ from basin to basin, but our recent methodological study, based on samples from the GYZ Formation, suggests that cut-offs of Mg/Ca < 0.4 g g^{-1}, Mn/Sr < 2 g g^{-1} and Sr/(Ca + Mg) > 200 μg g^{-1} are able to distinguish samples that record Sr isotope values closest to seawater composition in this formation (Chen and Zhou 2023).

The Sr isotope ratios (Chen *et al.* 2025) were measured on the same group of samples used in this study and from the same leachate as the REE data, which helps to rule out any differences caused by leaching. Applying the cut-offs for Mn/Sr, Mg/Ca and Sr/(Ca + Mg) used to select seawater Sr isotope data to screen REE and Ce anomalies (Fig. 6), we found that the screened samples do not necessarily contain seawater-like REE patterns (Fig. 7a) and do not reveal a stratigraphic Ce anomaly trend (Fig. 7d), similar to the results without screening. However, when REE data are screened using REE pattern parameters such as $Pr_N/Yb_N < 1$, La anomaly >1, $Dy_N/Sm_N > 1$ and Y/Ho > 35 (Fig. 6), as suggested by previous studies (Tostevin *et al.* 2016*b*; Zhang and Shields 2022), not only do the screened samples that meet all these thresholds display a seawater-like pattern with LREE depletion (Fig. 7b), but also the corresponding Ce anomalies show a negative shift (Fig. 7e) broadly coincident with the $\delta^{13}C$ excursion (Fig. 7f).

Two observations emerge from the above discussion: (1) the apparent difference in Ce anomaly trend between samples that have been screened and unscreened (for a seawater-like pattern) (Fig. 7e), and (2) inconsistency between samples with seawater-like Sr isotope values (Fig. 7d) and those with seawater-like REE patterns (Fig. 7e). If carbonate REE patterns resist diagenetic alteration (Banner *et al.* 1988), then screened and unscreened samples (Fig. 7e) should not exhibit significantly different stratigraphic trends. Moreover, samples with seawater-like Sr isotope ratios might be expected to also exhibit seawater-like REE patterns, given that Sr isotopes are considered to be more sensitive to diagenetic alteration than REE (Banner and Hanson 1990; Lau and Hardisty 2022). Our findings suggest that REE and Sr isotopes behave as two distinct diagenetic systems. The primary REE carriers, such as Mn or Fe oxides and organic matter, contain abundant REE but relatively low Sr concentrations compared to carbonate rocks. Thus, during diagenesis, carbonate REE patterns could be altered due to REE release into porewaters from these carriers, with Sr remaining unaffected. Detrital minerals, which have high concentrations of both Sr and REE, can also be dissolved and incorporated into carbonate minerals during diagenesis, thereby altering both Sr isotopes and REE patterns. However, the lack of covariation between Al, Rb and Si concentrations and REE patterns suggests that detrital contamination was not the primary control over REE patterns during the studied interval but may be a key factor influencing Sr isotopes (Chen *et al.* 2025), thus causing the inconsistency between samples with seawater-like Sr isotopes and REE patterns. Similarly, the different amount of screened samples for $\delta^{13}C$ and the Ce anomaly also reflect the distinct diagenetic sensitivities of these two proxies under various systems. While the dissolution of Fe–Mn oxides may coincide with organic matter degradation, early diagenetic porewaters were probably buffered by the large dissolved inorganic carbon pool in the Proterozoic ocean that would have helped preserve primary carbonate carbon isotope signatures (e.g. Zhang and Shields 2023). This decoupling is also evident in previous studies; for example, samples display well-preserved Sr and C isotope values in the Doushantuo Formation

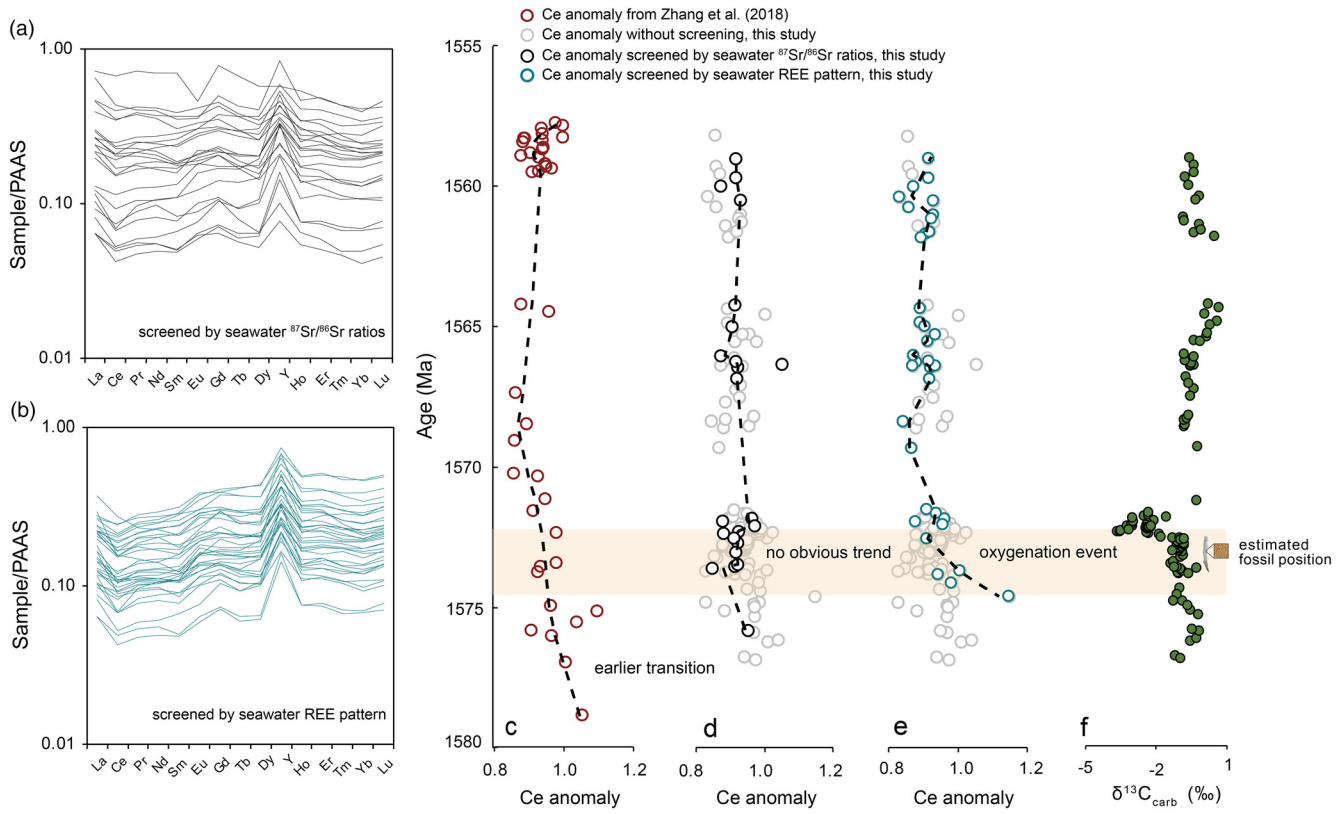

Fig. 7. Comparison of samples screened by seawater-like strontium isotopes and seawater-like rare earth element (REE) patterns for Ce anomaly. (**a**) Samples screened by seawater-like Sr isotopes using Mg/Ca, Sr/(Ca + Mg) and Mn/Sr (cut-off values shown in Fig. 6). (**b**) Samples screened by REE pattern parameters (cut-off values discussed in the text and Fig. 6). (**c**) Ce anomaly data from Zhang *et al.* (2018) showing an earlier transition from anoxic to oxic seawater (Ce anomaly <1) than this study in Figure 7e. The data of Zhang *et al.* (2018) have been normalized to post-Archean Australian Shale (PAAS) values of Pourmand *et al.* (2012), consistent with this study. (**d**) Samples from this study screened by seawater-like Sr isotopes show no trend for Ce anomaly. (**e**) Samples from this study screened by seawater-like REE patterns show a negative Ce anomaly during the C isotope excursion. (**f**) C isotope data from this study and the estimated position for the appearance of decimetre-scale, multicellular eukaryotic macrofossils (Zhu *et al.* 2016). The *y*-axis of (c)–(e) and (f) represents age in Ma. Age models and stratigraphic correlations are constructed based mainly on carbon isotope stratigraphy and published dating constraints. The beige box indicates the oxygenation event. Black dashed lines show the LOWESS fit curves with a smoothing factor of 0.2. Source: (c) Ce anomaly data from Zhang *et al.* (2018).

(Sawaki *et al.* 2010; Zhao *et al.* 2021) despite exhibiting non-seawater-like REE patterns (Zhao *et al.* 2021).

Evaluating the utility of the Ce anomaly as a redox proxy

Cross-plots are usually invoked to screen for primary Ce anomalies, which are commonly plotted against potential diagenetic proxies (Tostevin *et al.* 2016*a*; Zhang *et al.* 2018). Nevertheless, due to differences in elemental partition coefficients between minerals and fluids, and variable diagenetic fluid compositions, generalized geochemical thresholds (e.g. using Mn/Sr) may not be suitable for screening REE and Ce anomaly data (see 'Comparing diagenetically sensitive $^{87}Sr/^{86}Sr$ with REE patterns' above). No covariation is observed between diagenetic indicators (including oxygen isotopes) and Ce anomalies in any section of this study (Fig. 6h–l). If this lack of covariation is taken to be a sign of signal fidelity, then all measured data may be supposed to represent primary signals and no significant Ce anomaly trend emerges (Fig. 7, grey circles). In contrast, despite the absence of covariation, it is evident that some samples display non-seawater-like REE patterns attributable to early diagenesis. In other words, a lack of covariation with Ce anomalies does not fully exclude the possibility of alteration.

As discussed above, there are multiple possibilities, including early diagenesis, to induce non-seawater-like REE patterns in carbonate rocks. As a coherent group, alteration of the REE pattern would also affect the Ce anomaly (Zhang and Shields 2023). Thus, we suggest that indiscriminate use of Ce anomalies with non-seawater-like REE patterns should be avoided unless careful consideration is given to other possibilities. It appears that the most straightforward way to screen for Ce anomalies would be through REE patterns (Fig. 7). Although determining the exact REE pattern of ancient seawater can involve circular reasoning, modern seawater-like REE patterns have been preserved in multiple proxy records, including carbonates and banded iron formations, extending back to the Archean (Kamber and Webb 2001; Zhang and Shields 2022). This recurring pattern across diverse lithologies and geological timescales suggests that modern seawater-like REE distributions serve as a robust first-order screening tool. Additionally, apparent non-seawater-like patterns, such as the LREE over HREE enrichment seen in this study for stage III-1,2, are not evident in modern oceans, even under anoxic conditions. The lack of modern analogues validates sample screening based on more seawater-like REE patterns.

The screened Ce anomalies from samples that exhibit a seawater-like pattern in this study shift from ~1.2 to ~0.9 (Fig. 7e). The transition observed in our study comes relatively later than that found in a previous study of the Jixian section (Zhang *et al.* 2018; Fig. 7c). It should be noted that the single positive Ce anomaly below the CIE comes from the Pingquan section. Considering that the Ce anomaly is a local proxy, the discrepancy in Ce anomaly trends may arise from different sample locations, although different approaches in data screening might also resolve this discrepancy. The positive Ce anomaly (~1.2) observed in the lowest screened sample of the Pingquan section may be related to the operation of

Mn oxide recycling, which requires a certain amount of dissolved oxygen in shallow seawater (~10 μM; Tostevin *et al.* 2016*a*). If the shift of Ce anomaly reflects a genuine change to seawater redox conditions, it probably marks a redox transition towards more oxic conditions. The subsequent $\delta^{13}C$ excursion may reflect the accumulation of oxidants to levels sufficient to oxidize the dissolved organic matter (Rothman *et al.* 2003) pool and/or sustain lower organic burial rates.

Nonetheless, it appears that compared to the previous study (Zhang *et al.* 2018), the redox transition identified in this study using the screened Ce anomalies aligns more closely with the CIE and with the oxygenation event indicated by independent proxies, such as $\delta^{53}Cr$, $\delta^{98}Mo$, I/(Ca + Mg) and $\delta^{34}S_{CAS}$ (Shang *et al.* 2019; Luo *et al.* 2020; Tang *et al.* 2022; Xie *et al.* 2023; Xu *et al.* 2023). This oxygenation event correlates with the first appearance of decimetre-scale multicellular eukaryotic macrofossils (Zhu *et al.* 2016; Fig. 7f) and may suggest a potential link between oxygenation and biological evolution.

Conclusions

This multi-section case study of REE in the GYZ Formation reveals a systematic trend from LREE enrichment before and during the carbon isotope excursion to a more LREE-depleted, seawater like pattern in the post-excursion stage. Our findings indicate that ocean redox evolution alone cannot fully explain the higher normalized concentrations of LREE than HREE through the CIE. Instead, we highlight the influence of Fe/Mn oxide dissolution in porewaters during early diagenesis. This process occurred without necessarily altering Sr contents or Sr isotope ratios in the same carbonate rocks, highlighting the need for distinct diagenetic screening methods in REE studies. Traditional diagenetic indicators such as Mn/Sr, Sr/(Ca + Mg) and Mg/Ca, which are commonly used to evaluate geochemical proxies such as Sr isotopes, may not be suitable for REE screening. Our data demonstrate that pattern-related parameters (Pr_N/Yb_N, Dy_N/Sm_N, Y/Ho) offer a straightforward method to identify diagenetic alteration and for Ce anomaly screening. The Ce anomalies identified in this study, screened using seawater-like REE patterns, reveal a negative shift, which aligns closely with the CIE, basin oxygenation and the appearance of decimetre-scale multicellular eukaryotic macrofossils, underscoring a potential link between oxygenation and biological evolution during the early Mesoproterozoic Era.

Scientific editing by Alexey Kamyshny

Author contributions **XC**: conceptualization (lead), data curation (lead), investigation (lead), methodology (lead), writing – original draft (lead), writing – review & editing (equal); **YZ**: funding acquisition (equal), methodology (lead), supervision (lead), writing – review & editing (equal); **FB**: data curation (lead), investigation (lead), writing – review & editing (equal); **CM**: data curation (lead), investigation (lead), writing – review & editing (equal); **KZ**: conceptualization (lead), investigation (equal), validation (lead), writing – review & editing (equal); **GAS**: conceptualization (lead), funding acquisition (lead), investigation (lead), supervision (lead), validation (equal), writing – review & editing (lead)

Funding This work was funded by the Natural Environment Research Council (NE/P013643/1), Natural Environment Research Council (NE/P013643/1), Natural Environment Research Council (NE/R010129/1) and Dean's Prize of the Faculty of Mathematical and Physical Sciences (UCL).

Competing interests The authors declare that they have no known competing financial interests or personal relationships that could have appeared to influence the work reported in this paper.

Data availability All data generated or analysed during this study are included in this published article (and if present, its supplementary information files).

References

Bailey, T.R., McArthur, J.M., Prince, H. and Thirlwall, M.F. 2000. Dissolution methods for strontium isotope stratigraphy: whole rock analysis. *Chemical Geology*, **167**, 313–319, https://doi.org/10.1016/S0009-2541(99)00235-1

Banner, J.L. and Hanson, G.N. 1990. Calculation of simultaneous isotopic and trace element variations during water-rock interaction with applications to carbonate diagenesis. *Geochimica et Cosmochimica Acta*, **54**, 3123–3137, https://doi.org/10.1016/0016-7037(90)90128-8

Banner, J.L., Hanson, G.N. and Meyers, W.J. 1988. Rare earth element and Nd isotopic variations in regionally extensive dolomites from the Burlington-Keokuk Formation (Mississippian): implications for REE mobility during carbonate diagenesis. *Journal of Sedimentary Petrology*, **58**, 415–432, https://doi.org/10.1306/212F8DAA-2B24-11D7-8648000102C1865D

Barnes, B. 2023. *The Biogeochemical Cycling of Rare Earth Elements in the Modern and Ancient Oceans*. PhD Thesis, Penn State University.

Barrat, J.A., Bayon, G. and Lalonde, S. 2023. Calculation of cerium and lanthanum anomalies in geological and environmental samples. *Chemical Geology*, **615**, https://doi.org/10.1016/j.chemgeo.2022.121202

Bau, M. and Dulski, P. 1996. Distribution of yttrium and rare-earth elements in the Penge and Kuruman iron-formations, Transvaal Supergroup, South Africa. *Precambrian Research*, **79**, 37–55, https://doi.org/10.1016/0301-9268(95)00087-9

Bau, M., Schmidt, K., Koschinsky, A., Hein, J., Kuhn, T. and Usui, A. 2014. Discriminating between different genetic types of marine ferro-manganese crusts and nodules based on rare earth elements and yttrium. *Chemical Geology*, **381**, 1–9, https://doi.org/10.1016/j.chemgeo.2014.05.004

Brand, U., Azmy, K., Tazawa, J.I., Sano, H. and Buhl, D. 2010. Hydrothermal diagenesis of Paleozoic seamount carbonate components. *Chemical Geology*, **278**, 173–185, https://doi.org/10.1016/j.chemgeo.2010.09.010

Byrne, R.H. and Kim, K.H. 1990. Rare earth element scavenging in seawater. *Geochimica et Cosmochimica Acta*, **54**, 2645–2656, https://doi.org/10.1016/0016-7037(90)90002-3

Cao, C., Liu, X.M., Bataille, C.P. and Liu, C. 2020. What do Ce anomalies in marine carbonates really mean? A perspective from leaching experiments. *Chemical Geology*, **532**, 119413, https://doi.org/10.1016/j.chemgeo.2019.119413

Chen, X. and Zhou, Y. 2023. Effective leaching of argillaceous and dolomitic carbonate rocks for strontium isotope stratigraphy. *Geostandards and Geoanalytical Research*, **48**, 57–75, https://doi.org/10.1111/ggr.12531

Chen, X., Zhou, Y. *et al.* 2025. Enhanced weathering and its potential connection to ocean oxygenation and eukaryotic evolution at 1.57 Ga. *EarthArXiv*, preprint, https://doi.org/10.31223/X5CB3D

Corkeron, M., Webb, G.E., Moulds, J. and Grey, K. 2012. Discriminating stromatolite formation modes using rare earth element geochemistry: trapping and binding versus in situ precipitation of stromatolites from the Neoproterozoic Bitter Springs Formation, Northern Territory, Australia. *Precambrian Research*, **212–213**, 194–206, https://doi.org/10.1016/j.precamres.2012.04.019

Cox, G.M., Halverson, G.P. *et al.* 2016. Continental flood basalt weathering as a trigger for Neoproterozoic Snowball Earth. *Earth and Planetary Science Letters*, **446**, 89–99, https://doi.org/10.1016/j.epsl.2016.04.016

Cui, H., Kaufman, A.J. *et al.* 2020. Primary or secondary? A dichotomy of the strontium isotope anomalies in the Ediacaran carbonates of Saudi Arabia. *Precambrian Research*, **343**, 105720, https://doi.org/10.1016/j.precamres.2020.105720

De Baar, H.J.W., Bacon, M.P., Brewer, P.G. and Bruland, K.W. 1985. Rare earth elements in the Pacific and Atlantic Oceans. *Geochimica et Cosmochimica Acta*, **49**, 1943–1959, https://doi.org/10.1016/0016-7037(85)90089-4

Elderfield, H. and Greaves, M.J. 1982. The rare earth elements in seawater. *Nature*, **296**, 214–219, https://doi.org/10.1038/296214a0

Gao, L., Ltu, P., Yin, C., Zhang, C., Ding, X., Liu, Y. and Song, B. 2011. Detrital zircon dating of Meso- and Neoproterozoic rocks in North China and its implications. *Acta Geologica Sinica (English Edition)*, **85**, 271–282, https://doi.org/10.1111/j.1755-6724.2011.00397.x

German, C.R. and Elderfield, H. 1990. Application of the Ce anomaly as a paleoredox indicator: the ground rules. *Paleoceanography*, **5**, 823–833, https://doi.org/10.1029/PA005i005p00823

German, C.R., Holliday, B.P. and Elderfield, H. 1991. Redox cycling of rare earth elements in the suboxic zone of the Black Sea. *Geochimica et Cosmochimica Acta*, **55**, 3553–3558, https://doi.org/10.1016/0016-7037(91)90055-A

Gladney, E.S. and Roelandts, I. 1988. 1987 Compilation of elemental concentration data for USGS BHVO-1, MAG-1, QLO-1, RGM-1, SCo-1, SDC-1, SGR-1 and STM-1. *Geostandards Newsletter*, **12**, 253–362, https://doi.org/10.1111/j.1751-908X.1988.tb00053.x

Gladney, E.S., O'Malley, B.T., Roelandts, I. and Gills, T.E. 1987. *Standard Reference Materials: Compilation of Elemental Concentration Data for NBS Clinical, Biological, Geological, and Environmental Standard Reference Materials*. National Bureau of Standards, Washington, DC.

Gorokhov, I., Semikhatov, M., Baskakov, A., Kutyavin, E., Mel'Nikov, N., Sochava, A. and Turchenko, T. 1995. Sr isotopic composition in Riphean, Vendian, and Lower Cambrian carbonates from Siberia. *Stratigraphy and Geological Correlation*, **3**, 1–28.

Guo, H., Du, Y., Kah, L.C., Huang, J., Hu, C., Huang, H. and Yu, W. 2013. Isotopic composition of organic and inorganic carbon from the Mesoproterozoic Jixian Group, North China: implications for biological and oceanic evolution. *Precambrian Research*, **224**, 169–183, https://doi.org/10.1016/j.precamres.2012.09.023

Halverson, G.P., Dudás, F.Ö., Maloof, A.C. and Bowring, S.A. 2007. Evolution of the 87Sr/86Sr composition of Neoproterozoic seawater. *Palaeogeography, Palaeoclimatology, Palaeoecology*, **256**, 103–129, https://doi.org/10.1016/j.palaeo.2007.02.028

Hashim, M.S., Burke, J.E., Hardisty, D.S. and Kaczmarek, S.E. 2022. Iodine incorporation into dolomite: experimental constraints and implications for the iodine redox proxy and Proterozoic Ocean. *Geochimica et Cosmochimica Acta*, **338**, 365–381, https://doi.org/10.1016/j.gca.2022.10.027

Hood, A. van S. and Wallace, M.W. 2015. Extreme ocean anoxia during the Late Cryogenian recorded in reefal carbonates of Southern Australia. *Precambrian Research*, **261**, 96–111, https://doi.org/10.1016/j.precamres.2015.02.008

Kamber, B.S. and Webb, G.E. 2001. The geochemistry of late Archaean microbial carbonate: implications for ocean chemistry and continental erosion history. *Geochimica et Cosmochimica Acta*, **65**, 2509–2525, https://doi.org/10.1016/S0016-7037(01)00613-5

Kamber, B.S., Bolhar, R. and Webb, G.E. 2004. Geochemistry of late Archaean stromatolites from Zimbabwe: evidence for microbial life in restricted epicontinental seas. *Precambrian Research*, **132**, 379–399, https://doi.org/10.1016/j.precamres.2004.03.006

Koeppenkastrop, D. and De Carlo, E.H. 1993. Uptake of rare earth elements from solution by metal oxides. *Environmental Science and Technology*, **27**, 1796–1802, https://doi.org/10.1021/es00046a006

Kuznetsov, A.B., Semikhatov, M.A. and Gorokhov, I.M. 2018. Strontium isotope stratigraphy: principles and state of the art. *Stratigraphy and Geological Correlation*, **26**, 367–386, https://doi.org/10.1134/S0869593818040056

Lau, K.V. and Hardisty, D.S. 2022. Modeling the impacts of diagenesis on carbonate paleoredox proxies. *Geochimica et Cosmochimica Acta*, **337**, 123–139, https://doi.org/10.1016/j.gca.2022.09.021

Lawrence, M.G., Greig, A., Collerson, K.D. and Kamber, B.S. 2006. Rare earth element and yttrium variability in South East Queensland waterways. *Aquatic Geochemistry*, **12**, 39–72, https://doi.org/10.1007/s10498-005-4471-8

Lécuyer, C., Reynard, B. and Grandjean, P. 2004. Rare earth element evolution of Phanerozoic seawater recorded in biogenic apatites. *Chemical Geology*, **204**, 63–102, https://doi.org/10.1016/j.chemgeo.2003.11.003

Li, H., Zhu, S. *et al.* 2010. Zircon U-Pb dating on tuff bed from Gaoyuzhuang Formation in Yanqing, Beijing: further constraints on the new subdivision of the Mesoproterozoic stratigraphy in the northern North China Craton. *Acta Petrologica Sinica*, **26**, 2131–2140.

Liang, T., Bao, Z., Zhu, X., Guo, Y., Li, J. and Jones, B. 2020. Rare earth elements in dolostones and limestones from the Mesoproterozoic Gaoyuzhuang Formation, North China: implications for penecontemporaneous dolomitization. *Journal of Asian Earth Sciences*, **196**, 104374, https://doi.org/10.1016/j.jseaes.2020.104374

Lin, P.C. and Catling, D.C. 2024. The rare Earth element distribution in marine carbonates as a potential proxy for seawater pH on early Earth. *American Journal of Science*, **324**, 10, https://doi.org/10.2475/001c.118215

Lu, S., Yang, C., Li, H. and Li, H. 2002. A group of rifting events in the terminal paleoproterozoic in the North China Craton. *Gondwana Research*, **5**, 123–131, https://doi.org/10.1016/s1342-937x(05)70896-0

Lu, Z., Jenkyns, H.C. and Rickaby, R.E.M. 2010. Iodine to calcium ratios in marine carbonate as a paleo-redox proxy during oceanic anoxic events. *Geology*, **38**, 1107–110, https://doi.org/10.1130/G31145.1

Luo, J., Long, X., Bowyer, F. and Poulton, S. 2020. Pulsed oxygenation events preceded progressive oxygenation of the early Mesoproterozoic ocean. *Earth and Planetary Science Letters*, **559**, 1656–1656, https://doi.org/10.46427/gold2020.1656

Luo, J., Poulton, S.W. *et al.* 2025. High-resolution chemostratigraphy reveals a large $\delta^{13}C$ gradient in the ~1.56 Ga redox-stratified ocean. *Precambrian Research*, **422**, 107785, https://doi.org/10.1016/j.precamres.2025.107785

McArthur, J.M. 1994. Recent trends in strontium isotope stratigraphy. *Terra Nova*, **6**, 331–358, https://doi.org/10.1111/j.1365-3121.1994.tb00507.x

Mei, M. 2006. Origin of molar-tooth structure based on sequence-stratigraphic position and macroscopic features: example from mesoproterozoic Gaoyuzhuang formation at Jixian Section, Tianjin, North China. *Journal of China University of Geosciences*, **17**, 201–208, https://doi.org/10.1016/S1002-0705(06)60029-0

Miller, N., Johnson, P.R. and Stern, R.J. 2008. Marine versus non-marine environments for the Jibalah Group, NW Arabian shield: a sedimentologic and geochemical survey and report of possible metazoa in the Dhaiqa formation. *Arabian Journal for Science and Engineering*, **33**, 55–77.

Nothdurft, L.D., Webb, G.E. and Kamber, B.S. 2004. Rare earth element geochemistry of Late Devonian reefal carbonates, Canning Basin, Western Australia: confirmation of a seawater REE proxy in ancient limestones. *Geochimica et Cosmochimica Acta*, **68**, 263–283, https://doi.org/10.1016/S0016-7037(03)00422-8

Nozaki, Y., Zhang, J. and Amakawa, H. 1997. The fractionation between Y and Ho in the marine environment. *Earth and Planetary Science Letters*, **148**, 329–340, https://doi.org/10.1016/s0012-821x(97)00034-4

Ovchinnikova, G., Gorokhov, I. and Belyatskii, B. 1995. U-Pb systematics of pre-Cambrian carbonates: the Riphean Sukhaya Tunguska Formation in the Turukhansk Uplift, Siberia. *Lithology and Mineral Resources*, **30**, 525–536.

Planavsky, N., Bekker, A., Rouxel, O.J., Kamber, B., Hofmann, A., Knudsen, A. and Lyons, T.W. 2010. Rare earth element and yttrium compositions of Archean and Paleoproterozoic Fe formations revisited: new perspectives on the significance and mechanisms of deposition. *Geochimica et Cosmochimica Acta*, **74**, 6387–6405, https://doi.org/10.1016/j.gca.2010.07.021

Pourmand, A., Dauphas, N. and Ireland, T.J. 2012. A novel extraction chromatography and MC-ICP-MS technique for rapid analysis of REE, Sc and Y: revising CI-chondrite and Post-Archean Australian Shale (PAAS) abundances. *Chemical Geology*, **291**, 38–54, https://doi.org/10.1016/j.chemgeo.2011.08.011

Pourteau, A., Smit, M.A., Li, Z.X., Collins, W.J., Nordsvan, A.R., Volante, S. and Li, J. 2018. 1.6 Ga crustal thickening along the final Nuna suture. *Geology*, **46**, 959–962, https://doi.org/10.1130/G45198.1

Rimstidt, J.D., Balog, A. and Webb, J. 1998. Distribution of trace elements between carbonate minerals and aqueous solutions. *Geochimica et Cosmochimica Acta*, **62**, 1851–1863, https://doi.org/10.1016/S0016-7037(98)00125-2

Rothman, D.H., Hayes, J.M. and Summons, R.E. 2003. Dynamics of the Neoproterozoic carbon cycle. *Proceedings of the National Academy of Sciences of the United States of America*, **100**, 8124–8129, https://doi.org/10.1073/pnas.0832439100

Rue, E.L., Smith, G.J., Cutter, G.A. and Bruland, K.W. 1997. The response of trace element redox couples to suboxic conditions in the water column: deep-sea research part I. *Oceanographic Research Papers*, **44**, 113–134, https://doi.org/10.1016/S0967-0637(96)00088-X

Satkoski, A.M., Fralick, P., Beard, B.L. and Johnson, C.M. 2017. Initiation of modern-style plate tectonics recorded in Mesoarchean marine chemical sediments. *Geochimica et Cosmochimica Acta*, **209**, 216–232, https://doi.org/10.1016/j.gca.2017.04.024

Sawaki, Y., Ohno, T. *et al.* 2010. The Ediacaran radiogenic Sr isotope excursion in the Doushantuo Formation in the Three Gorges area, South China. *Precambrian Research*, **176**, 46–64, https://doi.org/10.1016/j.precamres.2009.10.006

Shang, M., Tang, D., Shi, X., Zhou, L., Zhou, X., Song, H. and Jiang, G. 2019. A pulse of oxygen increase in the early Mesoproterozoic ocean at ca. 1.57–1.56 Ga. *Earth and Planetary Science Letters*, **527**, 115797, https://doi.org/10.1016/j.epsl.2019.115797

Sholkovitz, E.R., Landing, W.M. and Lewis, B.L. 1994. Ocean particle chemistry: the fractionation of rare earth elements between suspended particles and seawater. *Geochimica et Cosmochimica Acta*, **58**, 1567–1579, https://doi.org/10.1016/0016-7037(94)90559-2

Tang, D., Fu, X. *et al.* 2022. Enhanced weathering triggered the transient oxygenation event at ~1.57 Ga. *Geophysical Research Letters*, **49**, e2022GL099018, https://doi.org/10.1029/2022GL099018

Tang, D., Fang, H. *et al.* 2023. Mesoproterozoic molar tooth structure related to increased marine oxygenation. *Journal of Geophysical Research: Biogeosciences*, **128**, e2022JG007077, https://doi.org/10.1029/2022JG007077

Tian, H., Zhang, J. *et al.* 2015. Zircon LA-MC-ICPMS U-Pb dating of tuff from Mesoproterozoic Gaoyuzhuang Formation in Jixian County of North China and its geological significance. *Acta Geoscientica Sinica*, **36**, 647–658.

Tostevin, R., Wood, R.A. *et al.* 2016*a*. Low-oxygen waters limited habitable space for early animals. *Nature Communications*, **7**, 12818, https://doi.org/10.1038/ncomms12818

Tostevin, R., Shields, G.A., Tarbuck, G.M., He, T., Clarkson, M.O. and Wood, R.A. 2016*b*. Effective use of cerium anomalies as a redox proxy in carbonate-dominated marine settings. *Chemical Geology*, **438**, 146–162, https://doi.org/10.1016/j.chemgeo.2016.06.027

Wallace, M.W., Hood, A., Shuster, A., Greig, A., Planavsky, N.J. and Reed, C.P. 2017. Oxygenation history of the Neoproterozoic to early Phanerozoic and the rise of land plants. *Earth and Planetary Science Letters*, **466**, 12–19, https://doi.org/10.1016/j.epsl.2017.02.046

Webb, G.E. and Kamber, B.S. 2000. Rare earth elements in Holocene reefal microbialites: a new shallow seawater proxy. *Geochimica et Cosmochimica Acta*, **64**, 1557–1565, https://doi.org/10.1016/S0016-7037(99)00400-7

Webb, G.E., Nothdurft, L.D., Kamber, B.S., Kloprogge, J.T. and Zhao, J.X. 2009. Rare earth element geochemistry of scleractinian coral skeleton during meteoric diagenesis: a sequence through neomorphism of aragonite to calcite. *Sedimentology*, **56**, 1433–1463, https://doi.org/10.1111/j.1365-3091.2008.01041.x

Weyl, P.K. 1960. Porosity through dolomitization: conservation-of-mass requirements. *SEPM Journal of Sedimentary Research*, **30**, https://doi.org/10.1306/74d709cf-2b21-11d7-8648000102c1865d

Wong, G.T.F. and Brewer, P.G. 1977. The marine chemistry of iodine in anoxic basins. *Geochimica et Cosmochimica Acta*, **41**, 151–159, https://doi.org/10.1016/0016-7037(77)90195-8

Xie, B., Zhu, J. *et al.* 2023. Mesoproterozoic oxygenation event: from shallow marine to atmosphere. *Bulletin of the Geological Society of America*, **135**, 753–766, https://doi.org/10.1130/B36407.1

Xu, D., Qin, Z., Wang, X., Li, J., Shi, X., Tang, D. and Liu, J. 2023. Extensive seafloor oxygenation during the early Mesoproterozoic. *Geochimica et Cosmochimica Acta*, **354**, 186–196, https://doi.org/10.1016/j.gca.2023.06.007

Zhang, K. and Shields, G.A. 2022. Sedimentary Ce anomalies: secular change and implications for paleoenvironmental evolution. *Earth-Science Reviews*, **229**, 104015, https://doi.org/10.1016/J.EARSCIREV.2022.104015

Zhang, K. and Shields, G.A. 2023. Early diagenetic mobilization of rare earth elements and implications for the Ce anomaly as a redox proxy. *Chemical Geology*, **635**, 121619, https://doi.org/10.1016/j.chemgeo.2023.121619

Zhang, S., Li, Z.X., Evans, D.A.D., Wu, H., Li, H. and Dong, J. 2012. Pre-Rodinia supercontinent Nuna shaping up: a global synthesis with new paleomagnetic results from North China. *Earth and Planetary Science Letters*, **353–354**, 145–155, https://doi.org/10.1016/j.epsl.2012.07.034

Zhang, K., Zhu, X.K. and Yan, B. 2015. A refined dissolution method for rare earth element studies of bulk carbonate rocks. *Chemical Geology*, **412**, 82–91, https://doi.org/10.1016/j.chemgeo.2015.07.027

Zhang, K., Zhu, X., Wood, R.A., Shi, Y., Gao, Z. and Poulton, S.W. 2018. Oxygenation of the Mesoproterozoic ocean and the evolution of complex eukaryotes. *Nature Geoscience*, **11**, 345–350, https://doi.org/10.1038/s41561-018-0111-y

Zhang, K., Miao, L., Zhang, S., Zhou, Y. and Shields, G. 2025. Persistent oxygenation of the Mesoproterozoic shallow ocean: evidence from the c. 1.44–billion-year-old Tieling Formation, North China Craton. *Journal of the Geological Society, London*, **183**, jgs2025-040, https://doi.org/10.1144/jgs2025-040.

Zhao, Y.Y., Zheng, Y.F. and Chen, F. 2009. Trace element and strontium isotope constraints on sedimentary environment of Ediacaran carbonates in southern Anhui, South China. *Chemical Geology*, **265**, 345–362, https://doi.org/10.1016/j.chemgeo.2009.04.015

Zhao, Y., Wei, W. *et al.* 2021. Rare earth element geochemistry of carbonates as a proxy for deep-time environmental reconstruction. *Palaeogeography, Palaeoclimatology, Palaeoecology*, **574**, 110443, https://doi.org/10.1016/j.palaeo.2021.110443

Zhou, Y., Pogge von Strandmann, P.A.E. *et al.* 2020. Reconstructing Tonian seawater $^{87}Sr/^{86}Sr$ using calcite microspar. *Geology*, **48**, 462–467, https://doi.org/10.1130/G46756.1

Zhu, S., Zhu, M. *et al.* 2016. Decimetre-scale multicellular eukaryotes from the 1.56-billion-year-old Gaoyuzhuang Formation in North China. *Nature Communications*, **7**, 11500, https://doi.org/10.1038/ncomms11500